THE ASTROPHYSICAL JOURNAL, 483:426–434, 1997 July 1

WAVELET ANALYSIS OF STELLAR CHROMOSPHERIC ACTIVITY VARIATIONS

P. FRICK,[1] S. L. BALIUNAS,[2] D. GALYAGIN,[1] D. SOKOLOFF,[3] AND W. SOON[2]

Received 1996 April 11; accepted 1997 January 27

ABSTRACT

Observations of chromospheric activity variations for some lower main-sequence stars from the Mount Wilson Observatory's HK project reveal a cyclic behavior comparable to the sunspot cycle. Even in the relatively short interval that they have been observed, those stars show stellar cycles and other features, like grand minima. The quasi-periodic nature of such variations is not completely compatible with the standard Fourier analysis, so we applied a wavelet analysis to study the nature of regularities in the data. We computed wavelet transforms and energy spectra for the 25 yr records of surface magnetic activity in four stars: HD 3651, HD 10700, HD 10476, and HD 201091. We present a modified wavelet technique that is suitable for analysis of data with gaps and find that the common aliasing problems due to the finite length of the observations and irregularly spaced gaps between data can be reduced on both large and small scales by applying this algorithm.

Subject headings: methods: numerical — stars: activity — stars: chromospheres — stars: magnetic fields — waves

1. INTRODUCTION

The dedicated program of observing Ca II H (396.8 nm) and K (393.4 nm) emission in stars on or near the lower main sequence (the Olin Wilson sample) at the Mount Wilson Observatory (MWO) has yielded a rich sample of stellar chromospheric variations (see, e.g., Baliunas et al. 1995; Baliunas & Soon 1995). A brief study of the records reveals that a significant fraction (i.e., about one-third) of stars exhibit normal stellar cycles comparable to the 11 yr sunspot cycle. Other recognizable features of variability from this database include Maunder minimum–type events, the transition to the Maunder minimum, double periods, and irregular variations (i.e., without obvious periodic cycles). From visual inspection of the MWO Ca II time series (e.g., Fig. 1 in Baliunas et al. 1995), one can easily estimate stellar activity periods for some of those cyclic variations without sophisticated data processing. However, in many other cases, a precise technique would be very useful in providing a complete quantitative description of stellar periodicities from these time series, especially since the length of the observed series is only a few times larger than that of the primary cycles.

The simplest technique available for investigating periodicities in astrophysical data is the Fourier analysis, i.e., the comparison between a record and a sinusoidal signal with a given frequency. However, the traditional Fourier transform method often may not be suitable for representing the real structure of observational data. This shortcoming is evident when the amplitude of the main periodicity changes with time and the sampling extends over a finite interval.

The application of Fourier analysis to such a record can lead to spurious periodicities. Therefore, a method of avoiding these artificial periodicities is needed, and wavelet transform is the technique advanced in this paper.

Several authors have applied the wavelet technique to solar activity data (e.g., Ochadlick, Kritikos, & Giegengack 1993; Nesme-Ribes et al. 1995; Lawrence, Cadavid, & Ruzmaikin 1995; Frick et al. 1997). The wavelet method can reveal small variations of the main period of solar activity (about 11 y; e.g., Frick et al. 1997). Foster (1996) recently discussed a rescaled wavelet-transform technique that was applied to study unevenly sampled light curves of the variable stars R Aquilae and FS Comae. This technique appears to be an effective method of reducing artificial periodicities resulting from Fourier analysis.

Two characteristics of the stellar chromospheric records complicate period analyses. The first is the limited duration of records (see Gilliland & Baliunas 1987 for a discussion on the objective characterization of stellar activity cycles under the constraint of finite intervals of observations). The second is the presence of gaps in the records (see, e.g., Fig. 1). These gaps are connected with practical constraints (e.g., seasonal window of observing opportunity, cloudy sky, telescope and/or facility refurbishments). Standard wavelet methods require time series to be regularly distributed in time. Any kind of interpolation may be used, but extended gaps in time series are difficult to fill by interpolation because the time interval covered by interpolation can be comparable to the duration of the observations in a year.

These constraints appear in the context of both Fourier and wavelet analysis. An extension of Fourier technique that attempts to circumvent one of those limitations is the Lomb-Scargle periodogram. Its aim is to correct the functional basis ($\cos \omega t$, $\sin \omega t$) of the Fourier transform to preserve its normalization condition on an uneven grid of times of observation. For this purpose, an extraction of the mean value of the signal under investigation and a phase shift of basis functions are used. The appealing features of the Lomb-Scargle normalized periodogram are that it does not require interpolation of missing data and that it weights data on a per-point rather than a per-time-interval basis.

In a way similar to that in which the Lomb-Scargle periodogram complements the Fourier method, we propose an extension of the wavelet transform technique. The adaptive wavelet method under consideration would apply to relatively short data series with gaps. The idea behind this method is basically the same as that behind the Lomb-Scargle periodogram: wavelet basis functions are corrected

[1] Institute of Continuous Media Mechanics, Korolyov Street, Building 1, 614061 Perm, Russia.
[2] Harvard-Smithsonian Center for Astrophysics, 60 Garden Street, Cambridge, MA 02138.
[3] Department of Physics, Moscow State University, 119899 Moscow, Russia.

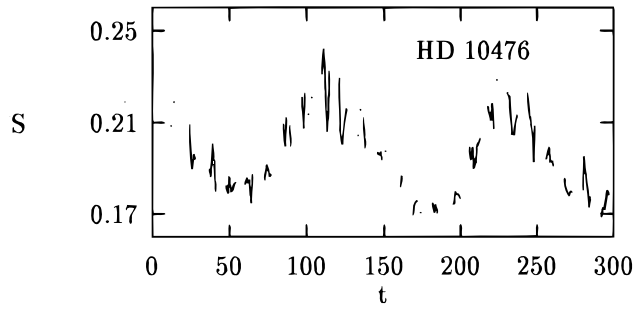

FIG. 1*a*

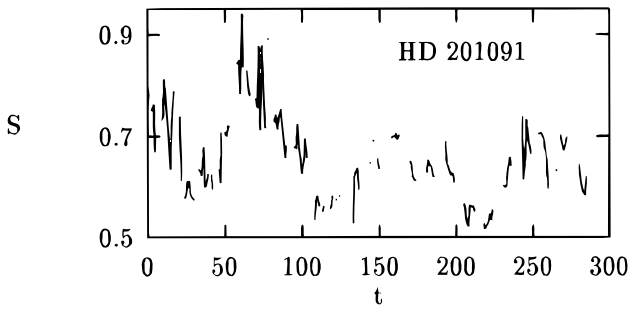

FIG. 1*b*

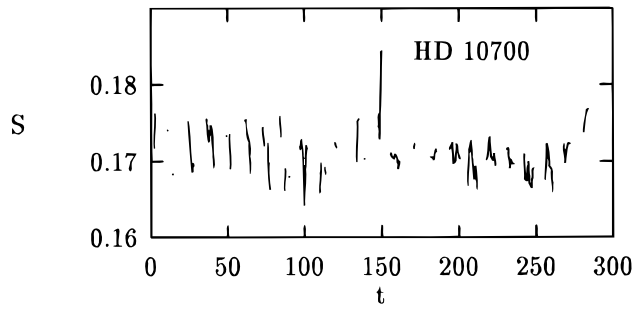

FIG. 1*c*

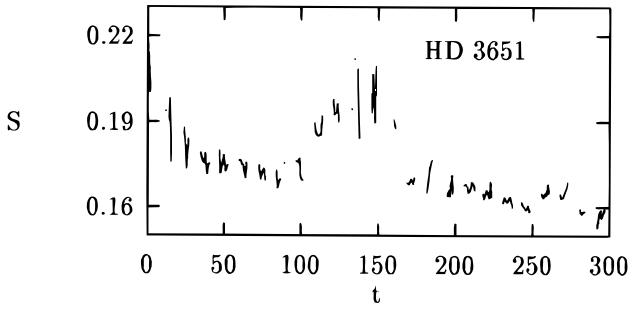

FIG. 1*d*

FIG. 1.—Records of Ca II activity variations, S (relative H and K emission fluxes), for (*a*) HD 10476, (*b*) HD 201091, (*c*) HD 10700, and (*d*) HD 3651. The time, t, is given in months. Strictly speaking, the observational data are a sample of isolated points, but to enhance visualization we connected all the points if the time between points was less than 1 month.

by an adaptive procedure to keep the admissibility condition on the uneven grid of discrete observations.

We were initially motivated to apply wavelet analysis to the stellar activity data. While performing this research, we were forced to develop an adaptive wavelet technique. As a result, the theoretical basis of adaptive wavelets must be verified. The suitability of the algorithms can be assessed by applying them to a systematic database like that from the MWO's HK project. We describe this technique and then compare the independent results from both the standard and adaptive wavelet transform techniques to previous periodicity searches performed on the stellar records with the Lomb-Scargle normalized periodogram method (Scargle 1982; Horne & Baliunas 1986).

Instead of the Lomb-Scargle periodogram method or the adaptive wavelet method, other signal-processing procedures like interpolation, extraction of long-term trend, etc., can be used. However, our proposed method provides a uniform procedure of data processing differing from ad hoc application of the latter. In addition, the wavelet transform allows the study of the variability of the main period over time and the study of the existence of multiscale processes as well as suppression of spectral noise and leakage, unlike the Fourier transform.

2. MWO HK PROJECT: MAGNETIC ACTIVITY OF LOWER–MAIN-SEQUENCE STARS

At MWO, chromospheric activity of 111 stars on or near the main sequence has been continuously monitored in two 1 Å flux bands centered on the Ca II H and K emission features, with the dedicated 60 inch (1.5 m) telescope (and the 100 inch [2.54 m] Hooker reflector during the 1966–1977 phase of the project) since 1966. This program was initiated by Wilson (1978; see also Vaughan, Preston, & Wilson 1978 for a description of the current spectrophotometer) and is known as the Mount Wilson HK project. The observed quantity, S, is the ratio of the fluxes in the narrow H and K passbands to those of two nearby 20 Å photospheric continuum passbands, R (centered at 400.1 nm) and V (centered at 390.1 nm), and is defined as

$$S = \alpha \frac{N_{\rm H} + N_{\rm K}}{N_R + N_V}, \tag{1}$$

where N denotes the photon counts in the four passbands of the spectrophotometer. The parameter, α, is a nightly calibration factor determined by measurements of standard stars and a standard lamp to account for potential long-term systematic instrumental drifts (Baliunas et al. 1995). Each of the four passbands is measured sequentially at a rapid rate, 30 Hz, and the total counts in each passband are corrected for sky and background illumination. The spectrum of a hollow cathode lamp is also used to correct for nightly Doppler shifts caused by a star's velocity relative to the Earth. The ratio of the two photospheric continuum fluxes, defined as the photometric index, $C_{RV} = 2.5 \log (N_R/N_V)$, is sensitive primarily to the effective stellar surface temperature and only weakly dependent on surface gravity and metal abundance for stars on the main sequence (Soon et al. 1993). Therefore, one can associate the time changes in the S-index to be primarily a reflection of intrinsic conditions of a star's chromosphere.

Physical interpretations of the variability detected in the Ca II H and K chromospheric emission fluxes as a time manifestation of stellar surface magnetic inhomogeneities have been discussed recently by Baliunas, Sokoloff, & Soon (1996b) and Baliunas et al. (1996a). Robust results on various features in the power spectra would shed light on the physical magnetic phenomena occurring on the surface

of the Sun and stars (e.g., characteristic perturbations by large-scale magnetic fields, radial and nonradial dynamical instabilities).

We apply the adaptive wavelet technique to study activity variations in HD 10476, HD 201091, HD 10700, and HD 3651. These stars were chosen to represent activity variations of pronounced stable cyclicity, cycles with changing periods, a Maunder minimum–type event, and perhaps, a transition to a Maunder minimum. Time series for these four stars are shown in Figure 1.

3. WAVELETS

Fourier analysis fails when one needs to consider the time dependence of spectral features. By contrast, wavelets are efficient in multiscale analysis. They have a localized, oscillatory form so that, unlike sinuosoids, they are localized near time t_0 and decay if $|t - t_0|$ exceeds the characteristic scale, a. Therefore, the wavelet representation can be considered to be a mathematical microscope with variable position and magnification. The wavelet transform represents one-dimensional signals as a function of both time and frequency (position and scale) and is similar to a local, filtered Fourier transform that can be obtained by dilating and translating the wavelet and then convolving it with the signal. The application and development of the wavelet-transform technique in signal processing has been rapid and extensive in the past decade; we simply refer the readers to several recent reviews and books (e.g., Farge 1992; Daubechies 1992; Holschneider 1995).

In general, a wavelet's family is generated from an analyzing wavelet, $\psi(t)$, by translations and dilations, such that

$$\psi_{a,b}(t) = a^{-1/2}\psi\left(\frac{t-b}{a}\right), \tag{2}$$

where a and b correspond to the dilation and translation scaling factors, respectively.

Some requirements must be met in order for the function $\psi(t)$ to be considered a wavelet. First, the function must have a zero mean (the *admissibility* condition):

$$\int_{-\infty}^{\infty} \psi(t)dt = 0 . \tag{3}$$

Second, the function should be localized in both physical and Fourier space (time and frequency); i.e., its time spread, Δt, and its frequency spread, $\Delta\omega$, must satisfy the condition $\Delta t\,\Delta\omega = \text{const}$. Because of the Heisenberg relation, this constant cannot be smaller than 2π and, for a given wavelet, actually has a slightly larger value.

As an illustration, we present two kinds of widely used wavelets: a real wavelet, called the Mexican hat,

$$\psi(t) = (1 - t^2)e^{-t^2/2} , \tag{4}$$

and a complex one, the Morlet wavelet,

$$\psi(t) = e^{-t^2/2}e^{i\omega_0 t} . \tag{5}$$

We shall adopt the Morlet wavelet with $\omega_0 = 6$ in all the following calculations.

The wavelet transform, $w(a, t)$, of a signal, $f(t)$, is defined as

$$w(a, t) = C_\psi^{-1/2}a^{-1/2}\int_{-\infty}^{\infty} \psi^*\left(\frac{t'-t}{a}\right)f(t')dt' , \tag{6}$$

where $\psi(t)$ is a real or complex analyzing wavelet and the asterisk denotes the complex conjugate. Here,

$$C_\psi = \int_{-\infty}^{\infty} |\omega|^{-1}\,|\hat{\psi}(\omega)|^2\,d\omega , \tag{7}$$

and $\hat{\psi}(\omega)$ is the Fourier transform of $\psi(t)$:

$$\hat{\psi}(\omega) = \int_{-\infty}^{\infty} \psi(t)e^{-i\omega t}\,dt . \tag{8}$$

In addition, at least one reconstruction formula is needed for recovering the signal from its wavelet coefficients and for deducing the energy (or other invariants). If $C_\psi < \infty$, the wavelet transform can be inverted (Grossmann & Morlet 1984) as

$$f(t) = C_\psi^{-1/2}\int_0^{\infty}\int_{-\infty}^{\infty} a^{-1/2}\psi\left(\frac{t-t'}{a}\right)w(a, t')\,\frac{dt'\,da}{a^2} . \tag{9}$$

An important property of the continuous wavelet transform is a generalization of Parseval's theorem (Grossmann & Morlet 1984):

$$\int_{-\infty}^{\infty} f_1(t)f_2^*(t)dt = C_\psi^{-1}\int_0^{\infty}\int_{-\infty}^{\infty} w_1(a, t)w_2^*(a, t)\,\frac{dt\,da}{a^2} . \tag{10}$$

The consequence is that it imposes equality between energy in physical and wavelet spaces.

The wavelet transform can also be related to the Fourier transform, $\hat{f}(\omega)$, of a signal $f(t)$ by

$$w(a, t) = C_\psi^{-1/2}a^{1/2}(2\pi)^{-1}\int_{-\infty}^{\infty} \hat{\psi}^*(a\omega)\hat{f}(\omega)e^{it\omega}\,d\omega , \tag{11}$$

and

$$\hat{f}(\omega) = C_\psi^{-1/2}\int_0^{\infty}\int_{-\infty}^{\infty} a^{1/2}\hat{\psi}(a\omega)w(a, t')e^{-it'\omega}\,\frac{dt'\,da}{a^2} . \tag{12}$$

The Fourier spectrum of a signal can be compared with the global wavelet spectrum, which is defined as the energy contained in all wavelet coefficients of the same scale a:

$$M(a) = \int |w(a, t)|^2\,dt . \tag{13}$$

This is related to the Fourier spectrum $E(\omega) = |\hat{f}(\omega)|^2$ by

$$M(a) \sim a\int E(\omega)\,|\hat{\psi}(a\omega)|^2\,d\omega . \tag{14}$$

For a strictly periodic signal, the wavelet spectrum is a smoothed version of the Fourier spectrum. Because of the normalization defined in equation (6), if the Fourier spectrum were to follow a power law, $E(\omega) \sim \omega^\alpha$, then the global wavelet spectrum will also display the same power-law relation, $M(a) \sim a^{-\alpha}$. However, for nonperiodic signals, the wavelet spectrum is no longer a smoothed version of the Fourier spectrum and equation (14) is invalid.

4. ADAPTIVE WAVELETS

As noted in § 1, the observational data series are of infinite length (sometimes so short that they contain only a few cycles of the main periodicity), and they may contain gaps of various sizes. Both kinds of limitations, denoted as the boundary and the gap problems, introduce common

hurdles for the application of standard wavelet analysis. Boundaries and gaps produce artifacts in the cone of influence, which extends to large timescales. To simplify notation, we consider a boundary or border as a semi-infinite gap.

The simplest procedure for a treatment of time series with gaps is interpolation. However, in the case in which gaps occupy an essential part of an observational interval, any smooth interpolation preceding spectral analysis can lead to an underestimation of power at higher frequencies. This condition is relevant for the chromospheric data we consider. Other treatments, like the extraction of the mean value, fail for signals with a trend. So a systematic method of treatment of time series with gaps is required.

Let us consider some stochastic or quasi-periodic signal, $f(t)$, that is known only in some intervals of time. Thus, we observe the function

$$f'(t) = f(t)G(t) , \tag{15}$$

where $G(t)$ is the function of data gaps, which is equal to 1 if the signal is registered and is equal to zero otherwise (i.e., in a gap or outside the window of observation). Instead of equation (6), one obtains

$$w'(a, t) = C_{\psi}^{-1/2} a^{-1/2} \int_{-\infty}^{\infty} \psi'^{*}\left(\frac{t' - t}{a}\right) f(t')dt' , \tag{16}$$

where

$$\psi'\left(\frac{t' - t}{a}\right) = \psi\left(\frac{t' - t}{a}\right)G(t') .$$

Near a gap, the function ψ' is used instead of the base wavelet, ψ, and consequently, ψ' will no longer satisfy the admissibility condition in equation (3), i.e.,

$$\int_{-\infty}^{\infty} \psi'\left(\frac{t' - t}{a}\right)dt' \neq 0 . \tag{17}$$

We carry the gap problem from the unknown function $f(t)$ to the well-known function ψ and replace the broken wavelet ψ' by an adaptive wavelet, $\tilde{\psi}$, which must satisfy (at least) the admissibility condition ($\langle\tilde{\psi}\rangle = 0$). The adaptive wavelet, $\tilde{\psi}$, approaches the initial wavelet, ψ, in the limit when the gap vanishes.

The proposed algorithm can be explained in terms of the spectral representation. The Fourier transform of the wavelet is localized in a band of frequencies, and it vanishes in the higher and lower frequencies. The loss of the admissibility condition means that $|\hat{\psi}'(\omega)|^2$ spreads in the low frequencies (up to $\omega = 0$). The singularities on the borders of the gap produce high-frequency noise. The proposed wavelet algorithm should suppress spurious frequencies in the spectrum at both high- and low-frequency limits.

To realize that idea, consider the analyzing wavelet, ψ, to be in the form

$$\psi(t) = h(t)\Phi(t) , \tag{18}$$

where $\Phi(t)$ is the positive-definite scale function [conveniently assumed to be the Gaussian $\Phi(t) = \exp(-t^2/2)$] and $h(t)$ represents the filling of the wavelet (e.g., the parabola in the Mexican hat, equation [4], or the complex harmonic function in the Morlet wavelet, equation [5]). The desired function, $\tilde{\psi}$, is written in the form

$$\tilde{\psi}(t', t, a) = \left[h\left(\frac{t' - t}{a}\right) - C(a, t)\right]\Phi\left(\frac{t' - t}{a}\right)G(t') . \tag{19}$$

The parameter C, which depends on dilation scale, a, and position of center of wavelet, t, could be obtained from the condition $\langle\tilde{\psi}\rangle = 0$ as

$$C(a, t) = \left[\int_{-\infty}^{\infty} \Phi\left(\frac{t' - t}{a}\right)G(t')dt'\right]^{-1} \times \int_{-\infty}^{\infty} h\left(\frac{t' - t}{a}\right)\Phi\left(\frac{t' - t}{a}\right)G(t')dt' . \tag{20}$$

The changes of a wavelet on a single gap are shown in Figure 2. We plot the Morlet wavelet only for those critical cases in which the gap covers exactly one positive half-

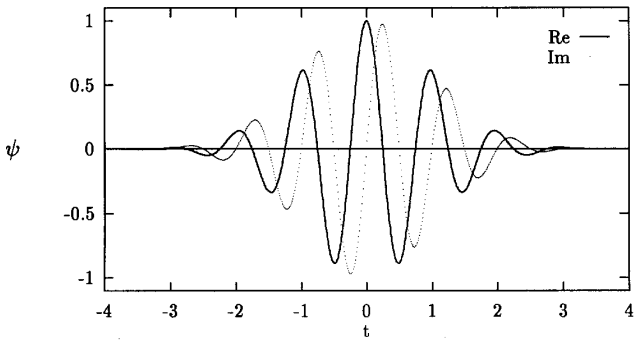

FIG. 2*a*

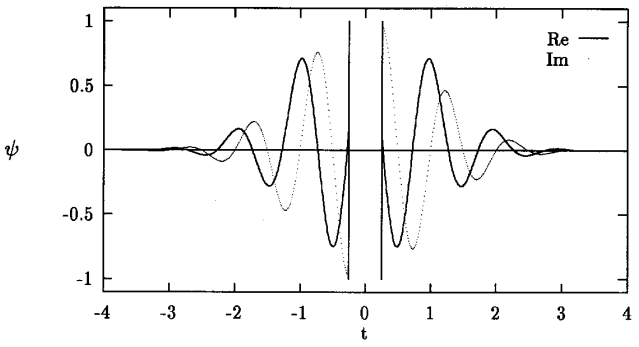

FIG. 2*b*

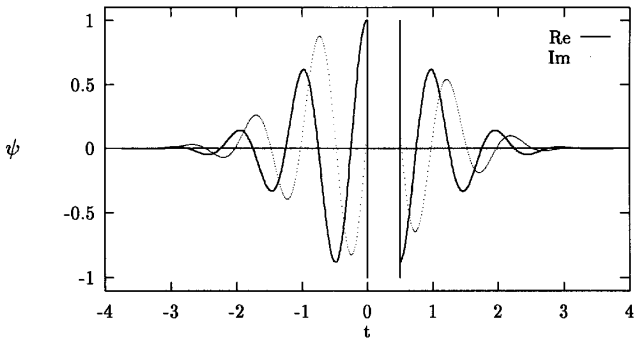

FIG. 2*c*

FIG. 2.—Examples of several wavelets. (*a*) Standard wavelet (Morlet wavelet), real (*solid lines*), and imaginary (*dashed lines*) parts. (*b*, *c*) Adaptive wavelet when the gaps cover one positive half-period of (*b*) cosine or (*c*) sine.

period of cosine or sine. The changes are less severe in other cases. The corrected basis functions are discontinuous, but the singularities arise on the borders of the gaps and do not produce new artifacts in the wavelet spectra of signals.

Let us compare adaptive wavelet technique results with that of Lomb-Scargle periodograms. The main features of the periodogram algorithm can be reiterated. First, the mean value of the signal is extracted. Second a frequency-dependent time offset (phase shift) is introduced. This time offset provides the zero mean value of basis functions on the given unevenly sampled data. Last, the basis functions are renormalized by their mean-square values on the same uneven sample of points. All of the steps can be considered to be corrections to the basis functions.

We modified the standard wavelet algorithm not by using a time offset (because the time offset is used to monitor time variability of the period) but rather by correcting the form of the basis function. Both the adaptive wavelet technique and the Lomb-Scargle periodogram lead to a significant enlargement of processor time. The Lomb-Scargle periodogram and the Fourier method in general give spectra with many peaks (see Fig. 4 and discussion below); some of them are artifacts of data processing. Wavelet transform tends to smooth these artificial peaks.

Examples that contain one dominant harmonic signal can illuminate the basic properties of the proposed algorithm in comparison to the standard wavelet analysis after simple interpolation. Three cases are discussed: (1) the gap is larger than the period, (2) the gap is of the same order as the period, and (3) the gap is smaller than the period. Only the adaptive technique is applicable to case (1) because interpolation cannot be performed in the case of a gap larger than the period. Case 1 is relevant to the determination of the rotation period of the Wilson sample stars because those periods are often shorter than observation seasonal gaps. Case 2 is the most difficult for both interpolation and adaptive algorithms. Case 3, which is the most interesting for applications to chromospheric data, is the most suitable for interpolation. However, even here adaptive algorithm has some advantages over interpolation. Real signals may have many spectral components, including pronounced high-frequency (or even white) noise; some of the frequencies are higher than or comparable to that of the gaps. The high-frequency part of the spectrum can be reconstructed only with the adaptive wavelet method.

The results for case 1 are presented in Figure 3. The left-hand panel (Fig. 3*a*) shows the time-frequency plot of the modulus of the wavelet transform $|w(a, t)|$ obtained by standard algorithm with the interpolation and mean-value subtraction discussed above, and the right-hand panel (Fig. 3*b*) plots the same quantity, but based on adaptive wavelets. The treated data series are indicated at the bottom of each panel. The main advantage of the adaptive algorithm is seen in the suppression of the large, dark clouds near the bottom of its time-frequency plot, which correspond to spurious power from large-scale oscillations.

5. WAVELET ANALYSIS OF STELLAR RECORDS

Our wavelet analysis of chromospheric activity data for four stars independently confirms the results of Baliunas et al. (1995), whose analysis was based on Lomb-Scargle periodograms. At the same time, the wavelet technique provides additional details concerning activity variations in these stars. In the present calculation of wavelet transforms, we used all the stellar Ca II data points as measured and no special data-filtering procedures. The previous period search analyses in Baliunas et al. (1995) were based on records using 30 day averages of these data points. As a result, minor differences may be expected in the exact numerical values of periods obtained in this paper compared with those from Baliunas et al. (1995).

As mentioned earlier, we applied the adaptive wavelet algorithm to four long-term records of stellar Ca II activity—HD 10476 (K2 V), HD 10700 (G8 V), HD 201091 (K5 V), and HD 3651 (K0 V). Figure 4 shows the integral wavelet spectra (indicated by thick solid lines in each panel),

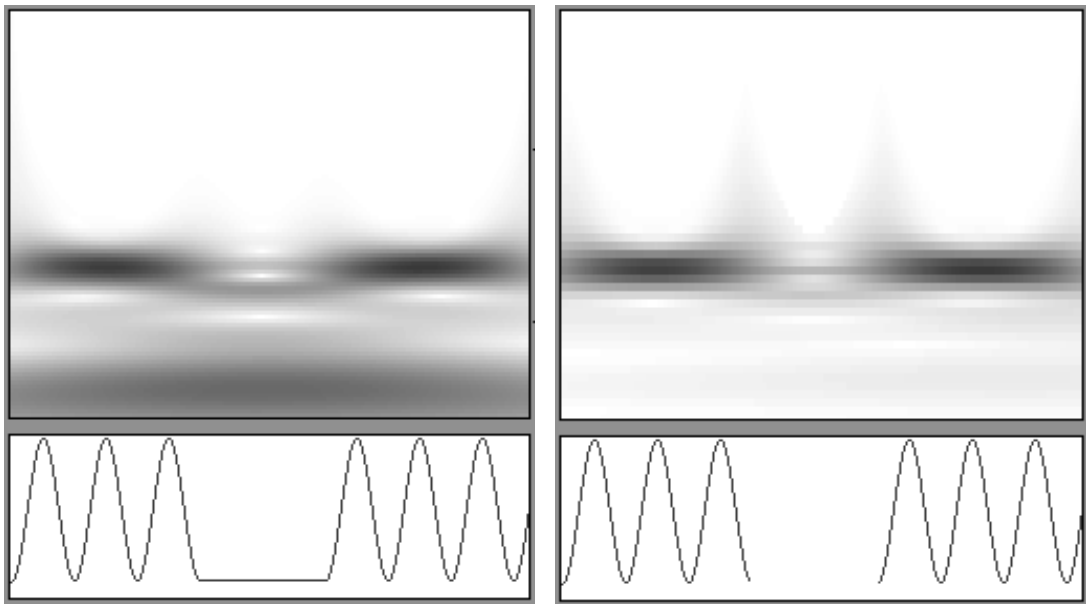

FIG. 3.—Comparison of the time-frequency plot of the modulus of wavelet coefficients for an artificial example, case 1, using the (*left*) standard and (*right*) adaptive wavelet algorithms.

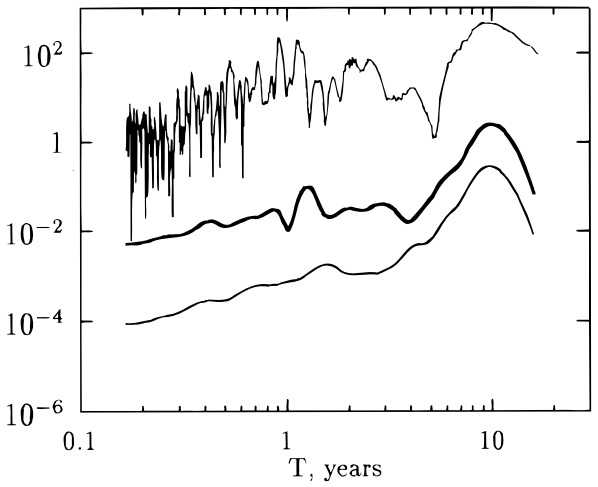

FIG. 4*a*

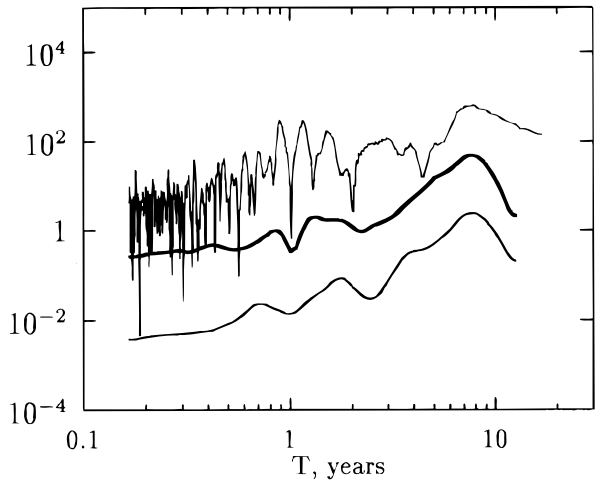

FIG. 4*b*

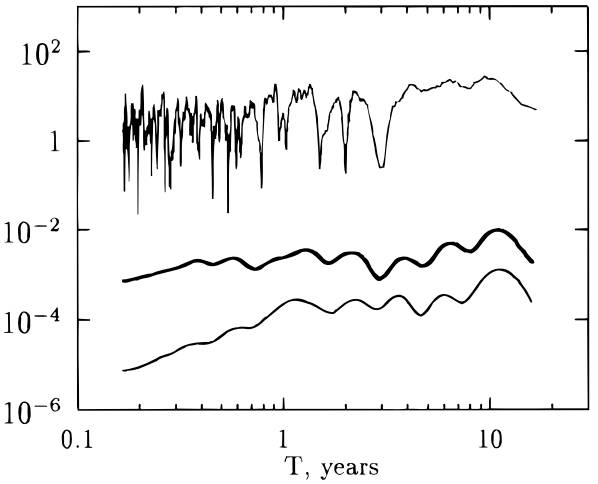

FIG. 4*c*

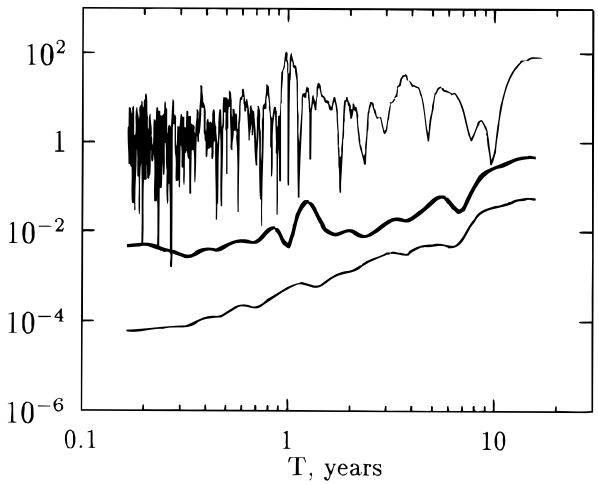

FIG. 4*d*

FIG. 4.—Comparison of wavelet spectra, plotted on log-log scales for four stars: (*a*) HD 10476; (*b*) HD 201091; (*c*) HD 10700; and (*d*) HD 3651. Values were calculated with the standard wavelet algorithm to the interpolated data (*thin lines at the bottom of each panel*), the adaptive wavelet algorithm (*thick lines in the center of each panel*), and the normalized spectral power calculated by Lomb-Scargle periodograms (*uppermost lines in each panel*). The three curves are plotted with an arbitrary vertical shift (2 orders of magnitude).

and Figure 5 shows the time frequency plot of the modulus of wavelet coefficients based on the adaptive wavelet algorithm. The activity records of these stars are representative of the variations found among the less active (hence, older) stars in the Wilson sample. HD 10476 and HD 201091 are examples of stars with prominent cycles (9.6 and 7.3 yr, respectively; Baliunas et al. 1995). HD 3651 has a less pronounced cycle of about 13.8 yr. HD 10700 is a star with a flat record of chromospheric activity.

We also present for comparison the integral wavelet spectra calculated using the standard wavelet technique for the interpolated data (lowermost lines in Figure 4) and the power spectra obtained from the Lomb-Scargle periodograms (uppermost lines in Fig. 4). All methods successfully found the main peak for HD 10476 and HD 201091. The spectral features obtained from the wavelet transform are less noisy. In contrast, many of the features in the Lomb-Scargle periodogram appear to be the result of spectral leakage and contamination. Both adaptive wavelets and periodogram techniques show relatively large power near the observational gaps of about 1 yr (excluding the case of HD 10700). That bias suggests that sampling at those scales is urgently needed before important physical questions related to the growth and decay of magnetically active regions can be addressed.

Comparing the two wavelet algorithms, one notes the pronounced decay of the standard wavelet spectrum at high frequency (for periods less than 1 yr), especially for HD 10700. This decay is a consequence of interpolation, which smooths the high frequencies in the data. Wavelet analysis based on interpolation underestimates the high-frequency contribution to the spectrum. In the case of HD 10700, standard wavelet analysis leads to the conclusion that the flat part of the spectrum covers timescales from 1 to 10 yr, while the adaptive wavelet transform extends that range to 0.1–10 yr. Such a bias arising from interpolation is impor-

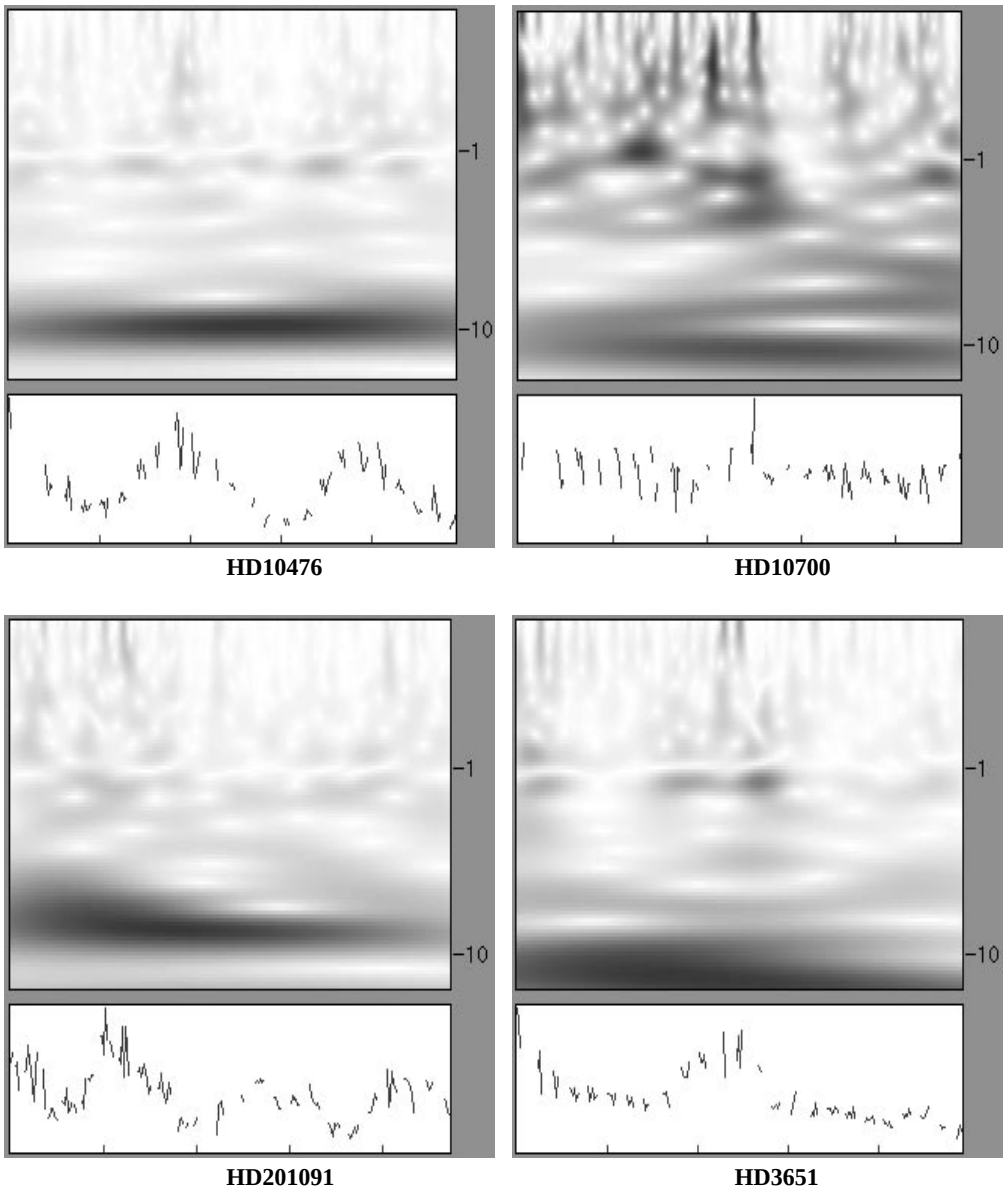

FIG. 5.—Time-frequency plot (frequency is plotted in years along the right-hand side of each panel) of the modulus of wavelet coefficients (*upper part of each panel*) for four stars: *top left*, HD 10476; *bottom left*, HD 201091; *top right*, HD 10700; and *bottom right*, HD 3651. Values were calculated with the adaptive wavelet algorithm. The original (uninterpolated) time series (in elapsed years) used for the analysis are shown at the bottom of each panel.

tant if one wants to deduce the correct physical picture for the nature of weak and low magnetic activity variations in HD 10700. The underestimation of high-frequency contributions by interpolation can also be seen for the other stars in Figure 4.

The modulus of wavelet coefficients is free of structure for HD 10476 (Fig. 5, *top left*). The integral spectrum (Fig. 4*a* contains only one dominant peak, corresponding to a period of 9.8 ± 1.5 yr. The uncertainty in the period is given by the full width at half-maximum of the main peak in the wavelet spectrum.

HD 201091 has a nominal periodicity of 7.5 ± 1.7 yr (Fig. 4*b*). The bottom left panel of Figure 5 shows that the actual activity variation is more complicated. The shortest period corresponds to the most intense oscillations at the beginning of the observational period. Later, the oscillations tend to be less intense while the period lengthens. This is denoted in Figure 5 (*bottom left*) by the changes in the dark layer drifting from short periods to longer periods while its intensity decreases. The upper range of observed periods for HD 201091 is about 10 yr. The changes of this period are not obvious from the results of the Lomb-Scargle technique.

HD 10700 has been classified as a star with flat temporal behavior; this result is supported by our wavelet results (Fig. 4*c*). However, from the available observational data, we cannot conclude whether its temporal variations can be characterized as pure white noise. Although there is a relatively pronounced, dark band on the wavelet time-frequency plot (Fig. 5, *top right*), the peak near 10 yr may not be significant because it is difficult to determine the noise level. A longer time series is needed to ascertain the absence of this periodicity.

HD 3651 was previously assigned a period of about 13.8 yr on the basis of the Lomb-Scargle periodogram. (We note that Baliunas et al. 1995 found the period of 13.8 yr to be significant only after a linear long-term trend in the data

series was removed.) The wavelet spectrum in the bottom right panel of Figure 5 indicates a broad peak near 14 yr. However, Figure 4*d* emphasizes that the available time series is too short to confirm the significance of this periodicity.

For the stars with well-pronounced cyclic behavior, HD 10476 and HD 201091, we analyzed the stability of the primary cycle by tracing the local maxima of spectral intensity, at a given instant of time, from the wavelet representation in Figure 5. We show the change in cycle length in Figure 6 (*solid lines*). The reliability of these period changes should be checked because spurious variations of the cycle period can appear when the wavelet transform is calculated on an unevenly sampled time series (Foster 1996). Presumably, these spurious period variations can arise because of beats between the frequency of the signal and the gaps. To check the significance of apparent period variation, we calculated the maximum of the wavelet transform of a pure sinusoid with the nominal period (indicated by dotted lines in Fig. 6) and phase as the main cycle in the time series. The results are given in Figure 6 by dot-dashed lines. We conclude from Figure 6*a* that the activity period of HD 10476 is stable in time because its apparent variations are of the same shape and order of magnitude as the variations connected by the irregularly sampled data.

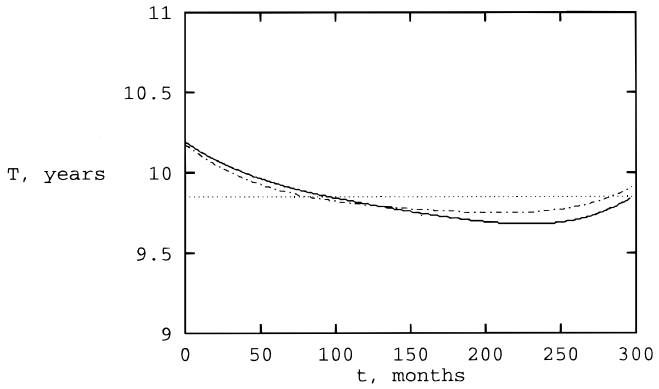

FIG. 6*a*

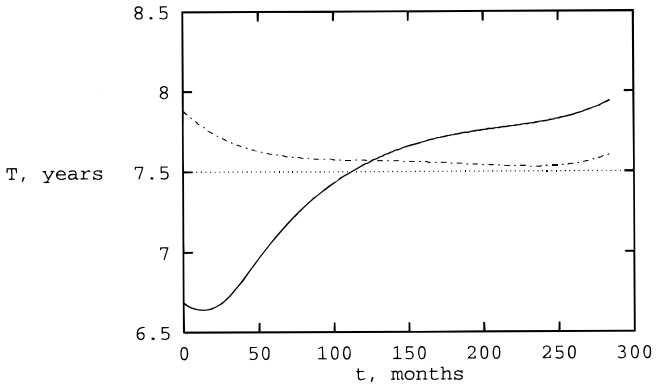

FIG. 6*b*

FIG. 6.—Changes in the length of the main period as a function of time for (*a*) HD 10476 and (*b*) HD 201091. The solid line indicates the result for the observed data. The dot-dashed line gives the result obtained by using the same algorithm for a pure sinusoid on the same sample of points as in the original stellar data. The horizontal line indicates the nominal period of the adopted sinusoid.

To the contrary, the variations of period of HD 201091 appear to be real because they are of dissimilar shape and much larger than variations of the sinusoidal signal produced by uneven sampling. Variations of the activity period in the record of HD 201091 are much more pronounced than in the Sun. Activity periods of HD 201091 vary with a range of about 25% from the mean, while the cycle intensity varies by a factor of about 2. The most pronounced deviations of the Schwabe cycle period (about 20%) are connected with the end of the Maunder minimum (e.g., Frick et al. 1997), while the cycle intensity (measured in units of weighted spot numbers) at that time was at least 10 times smaller than the average solar activity.

6. DISCUSSION

In the four stars we analyzed, results from the wavelet transform method are in basic agreement with those obtained from the Lomb-Scargle periodogram but reveal more details of variation. Thus, the adaptive technique can extend the standard wavelet method and yield additional information beyond that from the Lomb-Scargle periodogram in the analysis of periodicities in the Wilson Ca II records.

The adaptive wavelet technique helps to reduce the effects of two problems of the detection of periodicities in time series: the presence of gaps in time series and boundary effects due to the finite length of time series. Because observed periods are, as a rule, much longer (ca. 10 yr) than the typical gap length (ca. several months), the boundary problem is more pronounced in the Mount Wilson data set. These results suggest that a simple interpolation over seasonal gaps can yield reasonable results, provided that boundary effects are evaluated according to the adaptive algorithm.

The leading wavelet-analysis ideas applied here are basically the same as those of Foster (1996), who analyzed time series for light curves of the variable stars R Aquilae and FS Comae. The Foster algorithm uses a modified Morlet wavelet. Its idea is founded on an orthogonalization of projections of the three basis functions (the real and imaginary parts of the Morlet wavelet, as well as a constant) given on an uneven sample. Our method also involves a correction of basis functions to fulfill the admissibility condition in equation (3). However, our method is independent of a particular choice of analyzing wavelet. It is the minimal correction of the wavelet that makes it admissible on unevenly sampled data.

We are greatly saddened by the untimely death of our colleague Elizabeth Nesme-Ribes, who dedicated her work to the understanding of our Sun's changing magnetic field, especially during the Maunder minimum and the critical transition phases to and from the Maunder minimum. We are grateful to John Lawrence for a stimulating review of an earlier version of the manuscript. The partial support from the Civilian Research and Development Foundation (CRDF) under grant 322 and from the Russian Foundation of Basic Research (D. S., D. G., and P. F.) under grant 96-02-16252-a is acknowledged. The numerical simulations were made possible by grants from the Swedish Royal Academy of Science, Eriksson Foundation, and material support from the Royal Institute of Technology, Stockholm (NADA). D. S. acknowledges partial financial support of the National Research Council's COBASE program. We

are grateful for the selfless efforts of our colleagues at Mount Wilson Observatory. The observational program at MWO was supported by the Electric Power Research Institute; Mobil Foundation, Inc.; Texaco Foundation, Inc.; the Scholarly Studies Program and the Langley-Abbot Fund of the Smithsonian Institution; the American Petroleum Institute; and the Richard C. Lounsbery Foundation. The research was made possible by a collaborative agreement between the Carnegie Institution of Washington and the Mount Wilson Institute.

REFERENCES

Baliunas, S. L., et al. 1995, ApJ, 438, 269
Baliunas, S. L., Nesme-Ribes, E., Sokoloff, D., & Soon, W. 1996a, ApJ, 460, 848
Baliunas, S., Sokoloff, D., & Soon, W. 1996b, ApJ, 457, L99
Baliunas, S., & Soon, W. 1995, ApJ, 450, 896
Daubechies, I. 1992, Ten Lectures on Wavelets (Philadelphia: Soc. Ind. Appl. Math.)
Farge, M. 1992, Ann. Rev. Fluid Mech., 24, 395
Foster, G. 1996, AJ, 112, 1709
Frick, P., Galyagin, D., Hoyt, D., Nesme-Ribes, E., Schatten, K. H., Sokoloff, D., & Zakharov, V. 1997, A&A, in press
Gilliland, R. L., & Baliunas, S. L. 1987, ApJ, 314, 766
Grossmann, A., & Morlet, J. 1984, SIAM J. Math. Anal., 15, 723
Holschneider, M. 1995, Wavelets: Tool of Analysis (Oxford: Oxford Univ. Press)
Horne, J. H., & Baliunas, S. L. 1986, ApJ, 302, 757
Lawrence, J. K., Cadavid, A. C., & Ruzmaikin, A. A. 1995, ApJ, 455, 366
Nesme-Ribes, E., Frick, P., Sokoloff, D., Zakharov, V., Ribes, J. C., Vigouroux, A., Laclare, F. 1995, CR Acad. Sci. Paris, Ser. IIb, 321, 525
Ochadlick, A. R., Kritikos, H. N., & Giegengack, R. 1993, Geophys. Res. Lett., 20, 1471
Scargle, J. D. 1982, ApJ, 263, 875
Soon, W. H., Zhang, Q., Baliunas, S. L., & Kurucz, R. L. 1993, ApJ, 416, 787
Vaughan, A. H., Preston, G. W., & Wilson, O. C. 1978, PASP, 90, 267
Wilson, O. C. 1978, ApJ, 226, 379